This article has been accepted for publication in a future issue of this journal, but has not been fully edited. Content may change prior to final publication. Citation information: DOI10.1109/LAWP.2024.3385275, IEEE Antennas and Wireless Propagation Letters

Ultra-Wideband High-Efficiency Dual-Polarized Conformal Phase Array for Wireless Power Transfer

Zhan Chen, Wei Hu, Xiangbo Wang, Yuchen Gao, and Lehu Wen

***Abstract*—In this letter, a novel methodology to remove the common-mode resonance of tightly coupled arrays using two-set unit cell and conformal operation is presented, whereby the ultra-wideband dual-polarized conformal phase array is developed with high efficiency for wireless power transfer applications. Initially, a design method to shift the common-mode resonance of a tightly coupled array outside of the operating band using two-set unit cell and conformal operation is described, and a dual-polarized two-set unit cell of infinite array is proposed with ultra-wideband operation. Subsequently, the 8 × 8 dual-polarized two-set unit cells are designed to conform a cylindrical surface with a radius of 200 mm (1.3λ), resulting in a cylindrical-conformal tightly coupled array. Ultimately, an experimental prototype of the obtained conformal array was manufactured and measured. It achieves an operated bandwidth of 2.2~12.4 GHz (5.6:1) with active VSWRs < 3.0 within ±60° scanning range in E-/H-planes and the average efficiency > 70% for dual-polarized operation. The good correspondence between the measured results and the simulated results illustrates the feasibility of the presented conformal array. Such a balanced high-performance conformal phase array provides a perfect solution for wireless power transfer systems of various maneuverable platforms.**

***Index Terms*—Conformal array, common-mode resonance, high efficiency, ultra-wideband, wireless power transfer.**

I. Introduction

MICROWAVE wireless power transfer technology can achieve continuous wireless energy supply for electronic devices in different application situations, with the advantages of high power and long distance. The rectenna consisted of antenna and rectifying circuit is an essential component of wireless energy transmission system [1]. Phased array antenna is a preferred choice for rectifying antennas due to the inherent high gain and flexible beam coverage [2]. To increase the energy conversion efficiency, the rectifying phased array antenna needs to have the capability of high efficiency within dual-polarized wideband operation [3]-[5]. Meanwhile, for the requirements of various maneuverable platforms such as unmanned aerial vehicles, highly-integrated conformal designs for rectifying antenna are becoming a development trend [6].

Vivaldi antennas have ultra-wideband and high-efficiency operation characteristic, but its high profile makes it challenge to be conformal along the carrier surface for array applications [7] [8]. Presently, planar tightly coupled dipole arrays (TCDAs) are extensively reported as popular low-profile ultra-wideband arrays [9]-[17]. Although it can achieve impedance matching and wide-angle scanning capability under ultra-wideband by loading frequency selective surfaces [10] or ferrite [14] [15] to remove common-mode resonance, it can lead to the reduction of antenna efficiency, which in turn reduces the efficiency of the whole wireless system. The requirement to simplify the structure of TCADs to make them to conformality has led to the challenge that conformal TCADs have a difficult balance between structure and high operating performance [18]-[20].

In this letter, a conformal dual-polarized TCDA employing two-set unit cells is proposed using a new method of shifting out the common-mode resonance for the high-efficiency wireless power transfer in various maneuverable platforms. The major contributions include:

1) A formulation for the calculation of the common-mode resonance frequency of dual-polarized TCDA using two-set unit cells is presented and validated.
2) Shifting the common-mode resonance to higher frequencies by using conformal operation ensures the impedance matching characteristics of proposed arrays at large-angles scanning.
3) The presented conformal array achieves a perfect balance in structure and electrical performance.

II. Planar Infinite Array Implementation

A. Common-Mode Resonance of Two-Set Unit Cell

The common-mode resonance of unit cell for infinite array has been analyzed in [9]. The common-mode resonance characteristics of two-set unit cell for infinite array is developed in this letter. The topology diagram of planar dual-polarized infinite array from unit cell to two-set unit cell is shown in Fig. 1. For the unit cells, the common-mode resonance frequency in the dual-polarized operation follows:

$$f_1^{\mathrm{cm}} \approx \frac{c_0}{2D\sqrt{\epsilon_{\mathrm{r,eff}}}} \tag{1}$$

where D is the spacing of element for the planar dual-polarized infinite array, C_0 is the speed of light in a vacuum.

This work was supported in part by the National Natural Science Foundation of China under Grant No. 62201417, in part by the 111 Project of China. (*Corresponding author: Wei Hu*)

Zhan Chen, Wei Hu, Xiangbo Wang, and Yuchen Gao are with the National Key Laboratory of Antennas and Microwave Technology, Xidian University, Xi'an, Shaanxi 710071, China (e-mail: chenzhan@stu.xidian.edu.cn; weihu.xidian@ieee.org; xiangbowang@stu.xidian.edu.cn; gaoyuchen@xidian.edu.cn).

Lehu Wen is with the Department of Electronic and Electrical Engineering, Brunel University London, Uxbridge, UB8 3PH, United Kingdom. (e-mail: lehuwen@ieee.org).

This article has been accepted for publication in a future issue of this journal, but has not been fully edited. Content may change prior to final publication. Citation information: DOI10.1109/LAWP.2024.3385275, IEEE Antennas and Wireless Propagation Letters

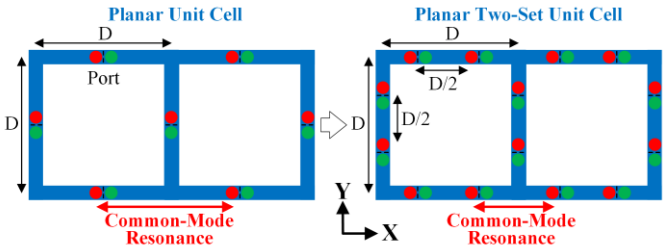

Fig. 1. Topology diagram of planar dual-polarized infinite array.

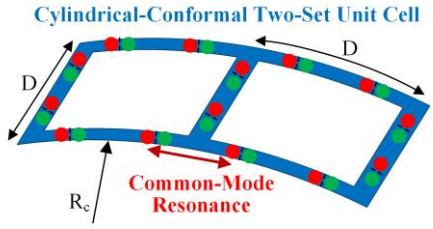

Fig. 2. Topology diagram of cylindrical-conformal dual-polarized infinite array using two-set unit cell.

$\epsilon_{r,eff}$ is the effective relative permittivity. If two-set unit cell design is used to operate together, the variation of the common-mode resonance frequency is obtained:

$$f_2^{cm} \approx \frac{c_0}{D\sqrt{\epsilon_{r,eff}}} \tag{2}$$

It can be easily found:

$$f_2^{cm} = 2\, f_1^{cm} \tag{3}$$

Because the distance D between the same-polarized ports is reduced to $D/2$. The frequency of common-mode resonance can be redoubled towards higher frequencies by increasing the number of feed ports within an element of infinite array.

In addition, the calculation of common-mode resonance frequency in cylindrical conformal array is also investigated as shown in Fig. 2. Here the spacing for calculating the common-mode resonance frequency is the straight length from the port rather than the arc length. Therefore, the frequency of common-mode resonance for the cylindrical-conformal array is obtained as following:

$$f_2^{cm} \approx \frac{c_0}{D\sqrt{\epsilon_{r,eff}}\cos(\frac{D}{R_c})} \tag{4}$$

where R_c is the curvature radius for the cylindrical conformal arrays. It is easily observed that the smaller R_c is, the higher the frequency at which the common-mode resonance appears.

B. Two-Set Unit Cell Design

The evolution processes of the proposed element are shown in Fig. 3. Dual-polarization of the proposed two-set unit cell is achieved by orthogonally combining two single-polarized elements. The full structure consists of power divider, balun, dipole, and wide-angle impedance matching (WAIM) layer. The Wilkinson power divider, connects to the dipole via a balun, is used not only to feed the dipoles of two-set unit cell, but also to implement an impedance transformation from 50 Ω to 100 Ω. The isolation resistance of the power divider is 100 Ω. The absence of common-mode resonance in the operating band allows the use of such a simple feed design. The

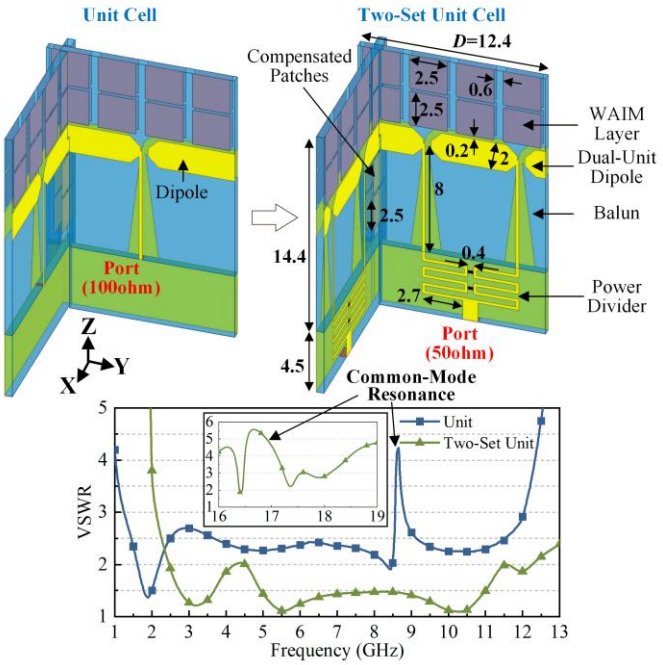

Fig. 3. Evolution processes of the proposed element of infinite array. (Dimensions are given in millimeters)

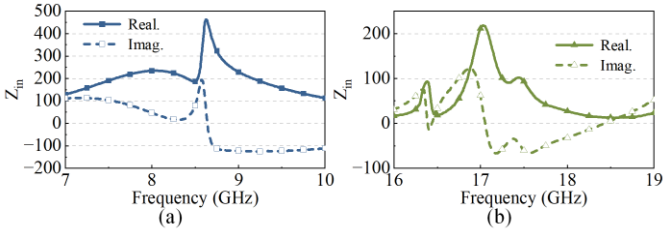

Fig. 4. Simulated active input impedance of (a) Unit cell. (b) Two-set unit cell.

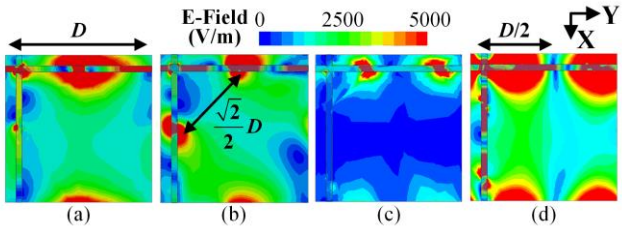

Fig. 5. Simulated E-field magnitudes of overhead view for infinite array. (a) Unit cell operated at 8.6 GHz. (b) Unit cell operated at 17.1 GHz. (c) Two-set unit cell operated at 8.6 GHz. (d) Two-set unit cell operated at 17.1 GHz.

compensated patches are loaded under the X-polarized dipole to improve the large-angle scanning capability. All metal is printed on both sides of the Rogers 4350 substrate (ε_r = 3.66) with the thickness of 0.508 mm. To better illustrate the impact of common-mode resonance on impedance matching, the simulated active input impedances of unit cell and two-set unit cell are displayed in Fig. 4. The dual-polarized unit cell of planar infinite array is first designed with common-mode resonance appearing near 8.6 GHz. Moreover, substituting the parameter of unit cell into (1) yields at this frequency f_1^{cm} = 9.1 GHz, which is quite nearly accurate within tolerance. The common-mode resonance frequency can be moved out of the operating band by designing of dual units with f_2^{cm} = 18.2 GHz computed by (2). The common-mode resonance of

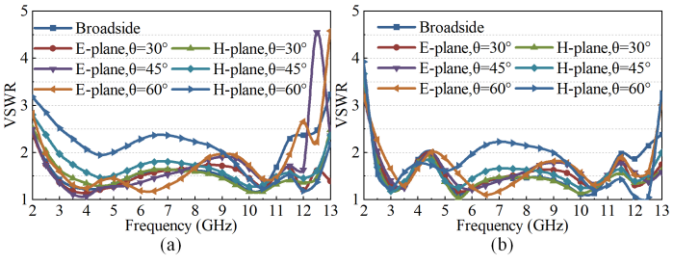

Fig. 6. Simulated infinite array active VSWRs for broadside, 30°, 45° and 60° scanning in the E- and H-planes. (a) X-polarization port operation. (b) Y-polarization port operation.

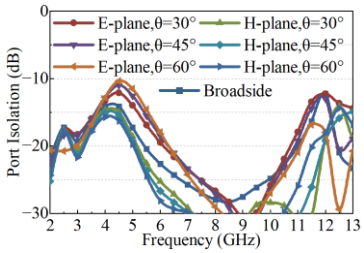

Fig. 7. Simulated port isolation for the proposed infinite array between the X- and Y-polarization input ports.

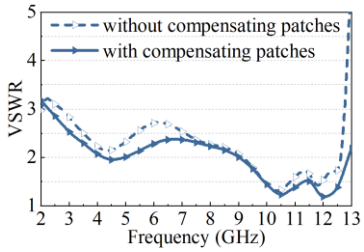

Fig. 8 Simulated infinite array active VSWRs of X-polarization port operation for 60° scanning in the H-planes with compensation patches and without compensation patches.

simulated results for the proposed two-set unit cell appears around 17.1 GHz, which agrees with the calculated results and is already far away from the observed band of 1~13 GHz. The active VSWR for the proposed two-set unit cell in infinite array is less than 2.5 in the operated band of 2.2~13.0 GHz. The two-set unit cell can shift the common-mode resonance more towards higher frequencies compared to conventional unit cells, which allow a wider operating band with high antenna efficiency.

The simulated E-field magnitudes of overhead view of unit cell and two-set unit cell in 8.6 GHz and 17.1 GHz are depicted in Fig. 5. From Fig. 5(a) and Fig. 5(d), the length of the common-mode resonance is reduced from *D* to *D*/2, which verifies the correctness of (3). For the unit cell operated at 17.1 GHz as shown in Fig. 5(b), there is a higher-order common-mode resonance outside the operating band [9]. For the two-set unit cell operated at 8.6 GHz in Fig. 5(c), there is no significant E-field of common-mode resonance generated.

C. Element Configuration and Performance

The simulated infinite array active VSWRs for broadside, 30°, 45° and 60° scanning in the E- and H-planes is shown in Fig. 6. The dual-polarized overlapping operating band is 2.2~12.2 GHz with active VSWRs < 3 and is 3.0~11.7 GHz with active VSWRs < 2.5. The simulated port isolation for the proposed infinite array between the X- and Y-polarization input ports is etched in Fig. 7. The port isolation is better than 10.3 dB within 60° scanning angles for the operating bands, which can ensure the radiation efficiency of the antenna, and keep a good validation of presented method.

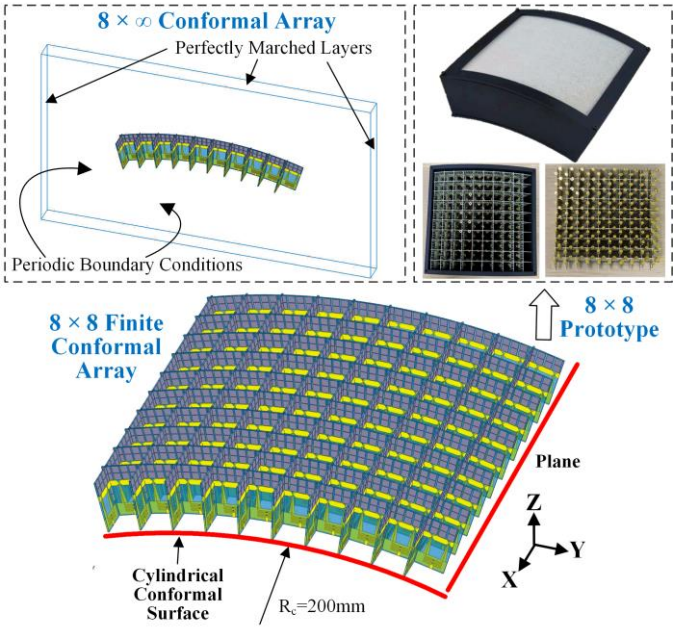

Fig. 9. Detailed configuration of the proposed cylindrical conformal array.

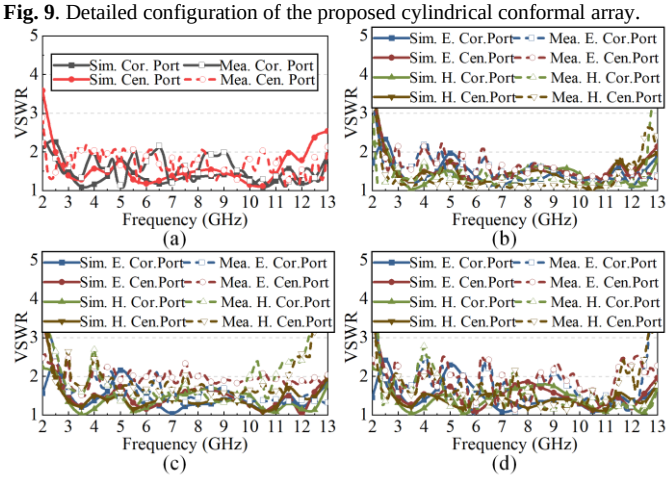

Fig. 10. Simulated and calculated active VSWRs of Y-polarized corner port and central port for the proposed conformal array. (a) Broadside. (b) 30° scanning. (c) 45° scanning. (d) 60° scanning.

To further illustrate the function of compensating patches, the simulated active VSWRs of X-polarization port operation for 60° scanning in the H-planes with compensation patches and without compensation patches are displayed in Fig. 8. In comparison, the loading of compensation patches can make the antenna have a better impedance matching when scanning to a large angle.

III. 8 × 8 Cylindrical Conformal Array

A. 8 × 8 Array Prototype

As shown in Fig. 9, a cylindrical conformal array is developed using the 8 × 8 dual-polarized two-set unit cells mounted on the cylindrical surface with the radius of 200 mm.

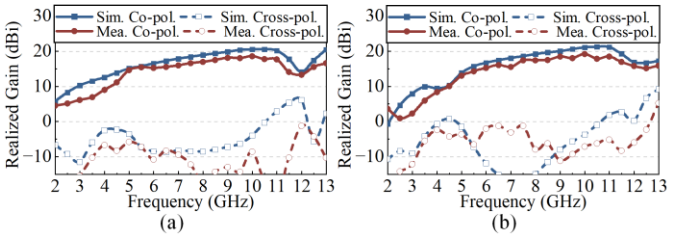

Fig. 11. Simulated and measured gains in broadside for the proposed conformal array. (a) X-polarization operation. (b) Y-polarization operation.

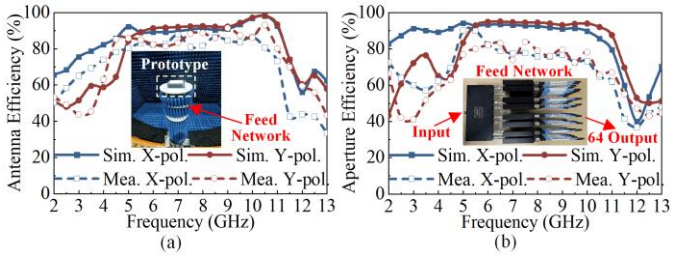

Fig. 12. Simulated and measured efficiencies in broadside for the proposed conformal array. (a) Antenna efficiency. (b) Aperture efficiency.

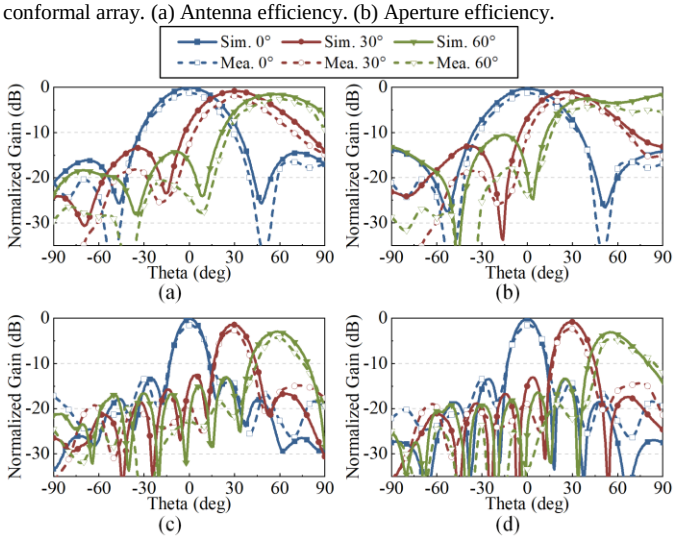

Fig. 13. Simulated and calculated normalized patterns of Y-polarization operation for the proposed conformal array. (a) 4 GHz at E-plane. (b) 4 GHz at H-plane. (c) 10 GHz at E-plane. (d) 10 GHz at H-plane.

It is important to note that the performance of a two-set unit cell in the conformal array be different from the planar infinite array. To accelerate the optimization process, simulation of 1 × 8 one-dimensional finite conformal arrays are verified before the design of 8 × 8 conformal arrays. For the sake of the brevity of this paper, the results of the tedious optimization are not given here. Finally, an 8 × 8 conformal array prototype is fabricated to verify the simulated design.

The simulated and measured active VSWRs of Y-polarized corner port and central port for the proposed 8 × 8 cylindrical conformal array are displayed in Fig. 10. The measured active VSWRs are obtained by summing S-parameters [18]. The active VSWRs are less than 3 between 2.2~12.4 GHz within 60° scanning range. Since this array conformality leads to a distance reduction from D to $D{\cdot}\cos(D/R_c)$ in the elements spacing, according to (4), the common-mode resonance frequency will be shifted to a higher frequency, so that no common-mode resonance will be introduced in the operating band during large-angle scanning.

TABLE I
COMPARISON WITH PREVIOUS CONFORMAL TIGHTLY COUPLED ARRAY

Ref.	BW*	Scan Range	Pol.*	Element Size (λ*)	Curvature Radius
[18]	3:1	±60° E. ±60° H.	Single	0.15×0.15×0.15	150mm (3λ)
[19]	2:1	±60° E. ±60° H.	Single	0.24×0.24×0.10	250mm (5λ)
[20]	9:1	Broadside	Single	0.06×0.06×0.05	200mm (1.3λ)
Pro.	**5.6:1**	**±60° E. ±60° H.**	**Dual**	**0.09×0.09×0.13**	**200mm (1.4λ)**

BW*: Bandwidth.
Pol.*: polarization.
λ* is the wavelength of the lowest operating frequency in free space.

A feed network of 64-way consisting of 9 8-way power dividers, 8 SMA male connectors, and 64 SMA to SSMP cables is used to feed the fabricated prototype. Then, the gains and efficiencies of proposed prototype in broadside are measured, where the insertion loss of the feed network was compensated in the measured results. Fig. 11 demonstrates the simulation results are similar to the measured results for the co-polarized gain in dual polarization operation. The cross-polarization has some effect due to interference from external noise. The simulated and measured efficiencies of proposed 8 × 8 conformal array are given in Fig. 12, which has a measured average antenna efficiency of 70.9% and average aperture efficiency of 72.6% in the operating band of 2.2~12.4 GHz. The aperture efficiency is calculated from the projected area of the proposed conformal array.

The simulated and measured normalized patterns of Y-polarization operation at 4 GHz and 10 GHz are shown in Fig.13. The gain variation is less than 3.0 dB in E-plane 60° scanning and 3.6 dB in H-plane 60° scanning. The difference is because the array is conformal along the Y-direction. Note that the calculated normalized patterns of the fabricated prototype are obtained by using active element pattern [19].

B. Comparisons

As list in Table I, a wider operating bandwidth is obtained compared to these antennas proposed in [18] and [19] due to the use of a two-set unit cell design that shifts the common-mode resonance frequency farther away from the operating band. Although a similar curvature conformal array achieves an operating bandwidth of 9:1, the single-polarized and broadside radiating characteristics limit its applications [20]. The conformal array presented in this letter achieves a perfect balance in structure and electrical performance.

IV. CONCLUSION

This letter presented a novel method for designing ultra-wideband high-efficiency dual-polarized conformal phase array by employing two-set unit cells remove common-mode resonance. The proposed conformal array with dual-polarized operation achieves an average efficiency more than 70.9% over a 5.6:1 operating band due to the shifting out of the common-mode resonance and achieves ±60° scanning in both principal planes, which is suitable for wireless power transfer applications in various maneuverable platforms.

REFERENCES

[1] N. Shinohara; J. Zhou, *Far-Field Wireless Power Transfer and Energy Harvesting*, Art., 2022.

[2] J. H. Kim, H. Y. Yu and C. Cha, "Efficiency Enhancement Using Beam Forming Array Antenna for Microwave-Based Wireless Energy Transfer," *2014 IEEE Wireless Power Transfer Conference*, Jeju, Korea (South), 2014, pp. 288–291.

[3] S. B. Liu, F. S. Zhang, M. Boyuan, S. P. Gao, and Y. X. Guo, "Multiband Dual-Polarized Hybrid Antenna With Complementary Beam for Simultaneous RF Energy Harvesting and WPT," *IEEE Trans. Antennas Propag.*, vol. 70, no. 9, pp. 8485–8495, Sep. 2022.

[4] Y. Huang, J. Zhou, and L. Li, "Wireless Power Transfer and Energy Harvesting Using Metamaterials and Metasurfaces," *2022 International Workshop on Antenna Technology (iWAT)*, Dublin, Ireland, 2022, pp. 280–283.

[5] B. Ma, J. Pan, S. Huang, S. Liu, T Ngo, Z. T. Aung, and Y. X. Guo, "Compact Dual-Polarized Antenna With Enlarged Effective-to-Physical Aperture Ratio for Wireless Power Transfer and RFID," *IEEE Trans. Antennas Propag.*, vol. 69, no. 7, pp. 4166–4171, Jul. 2021.

[6] N. Takabayashi, N. Shinohara, T. Mitani, M. Furukawa, and T. Fujiwara, "Rectification Improvement With Flat-Topped Beams on 2.45-GHz Rectenna Arrays," *IEEE Trans. Microwave Theory Techn.*, vol. 68, no. 3, pp. 1151–1163, Mar. 2020.

[7] X. Shi, Y. Cao, Y. Hu, X. Luo, H. Yang, and L. H. Ye, "A High-Gain Antipodal Vivaldi Antenna With Director and Metamaterial at 1–28 GHz," *IEEE Antennas Wireless Propag. Lett.*, vol. 20, no. 12, pp. 2432–2436, Dec. 2021.

[8] Y. Chen, Y. He, W. Li, L. Zhang, S. W. Wong, and A. Boag, "A 3–9 GHz UWB High-Gain Conformal End-Fire Vivaldi Antenna Array," *2021 IEEE International Symposium on Antennas and Propagation and USNC-URSI Radio Science Meeting (APS/URSI)*, Dec. 2021, pp. 737–738.

[9] S. S. Holland and M. N. Vouvakis, "The Banyan Tree Antenna Array," *IEEE Trans. Antennas Propag.*, vol. 59, no. 11, pp. 4060–4070, Nov. 2011.

[10] E. Yetisir, N. Ghalichechian, and J. L. Volakis, "Ultrawideband Array With 70° Scanning Using FSS Superstrate," *IEEE Trans. Antennas Propag.*, vol. 64, no. 10, pp. 4256–4265, Oct. 2016.

[11] Y. Zhou, F. Zhu, S. Gao, Q. Luo, L. H. Wen, Q. Wang, X. Yang, Y. Geng, and Z. Cheng, "Tightly Coupled Array Antennas for Ultra-Wideband Wireless Systems," *IEEE Access*, vol. 6, pp. 61851–61866, 2018.

[12] R. N. Pack, A. S. Brannon, and D. S. Filipovic, "Tightly Coupled Array of Horizontal Dipoles Over a Ground Plane," *IEEE Trans. Antennas Propag.*, vol. 68, no. 3, pp. 2097–2107, Mar. 2020.

[13] C. H. Hu, B. Z. Wang, G. F. Gao, R. Wang, S. Q. Xiao, and X. Ding, "Conjugate Impedance Matching Method for Wideband and Wide-Angle Impedance Matching Layer With 70° Scanning in the H-Plane," *IEEE Antennas Wireless Propag. Lett.*, vol. 20, no. 1, pp. 63–67, Jan. 2021.

[14] B. Wang, S. Yang, Z. Zhang, Y. Chen, S. Qu, and J. Hu, "A Ferrite-Loaded Ultralow Profile Ultrawideband Tightly Coupled Dipole Array," *IEEE Trans. Antennas Propag.*, vol. 70, no. 3, pp. 1965–1975, Mar. 2022.

[15] L. Li, J. B. Yan, C. O'Neill, C. D. Simpson, and S. P. Gogineni, "Coplanar Side-Fed Tightly Coupled Ultra-Wideband Array for Polar Ice Sounding," *IEEE Trans. Antennas Propag.*, vol. 70, no. 6, pp. 4331–4341, Jun. 2022.

[16] D. M. Sun, Z. C. Hao, W. Y. Liu, and C. Y. Ding, "An Ultrawideband Dual-Polarized Phased Array Antenna for Sub-3–GHz 5G Applications With a High Polarization Isolation," *IEEE Trans. Antennas Propag.*, vol. 71, no. 5, pp. 4055–4065, May 2023.

[17] H. Wang, S. W. Qu, S. Yang, and J. Hu, "Low-Profile Planar Ultrawideband Modular Antenna Array Loaded With Parasitic Metal Strips," *IEEE Trans. Antennas Propag.*, vol. 71, no. 7, pp. 5805–5816, Jul. 2023.

[18] S. Xiao, S. Yang, H. Zhang, Q. Xiao, Y. Chen, and S. W. Qu, "Practical Implementation of Wideband and Wide-Scanning Cylindrically Conformal Phased Array," *IEEE Trans. Antennas Propag.*, vol. 67, no. 8, pp. 5729–5733, Aug. 2019.

[19] S. Hussain, S. W. Qu, P. Zhang, X. H. Wang, and S. Yang, "A Low-Profile, Wide-Scan, Cylindrically Conformal *X* -Band Phased Array," *IEEE Antennas Wireless Propag. Lett.*, vol. 20, no. 8, pp. 1503–1507, Aug. 2021.

[20] X. Chen and K. Li, "Ultrathin and Flexible Ultrawideband Antenna Array Based on Integrated Impedance Matching Line," *IEEE Antennas Wireless Propag. Lett.*, vol. 22, no. 5, pp. 960–964, May 2023.